CrossMark

Isotopic Signatures of Supernova Nucleosynthesis in Presolar Silicon Carbide Grains of Type AB with Supersolar ^{14}N/^{15}N Ratios

Peter Hoppe [1], Richard J. Stancliffe[2,6], Marco Pignatari[2,3,4,6], and Sachiko Amari[5]
[1] Max Planck Institute for Chemistry, Hahn-Meitner-Weg 1, D-55128 Mainz, Germany; peter.hoppe@mpic.de
[2] E. A. Milne Centre for Astrophysics, University of Hull, HU6 7RX, Hull, UK
[3] Konkoly Observatory, Konkoly Thege Miklos ut 15-17, 1121, Budapest, Hungary
[4] Joint Institute for Nuclear Astrophysics—Center for the Evolution of the Elements (JINA-CEE), USA
[5] McDonnell Center for the Space Sciences and Physics Department, Washington University, St. Louis, MO 63130, USA

Abstract

We report high-resolution C, N, Al, Si, and S isotope data of 38 presolar SiC grains of type AB. Seventeen of these grains are of subtype AB1 (^{14}N/^{15}N < 440 = solar) and 20 of subtype AB2 (^{14}N/^{15}N ⩾ 440), previously proposed to be mainly from supernovae (AB1) and J-type carbon stars (AB2), respectively. Our data are compatible with previously obtained isotope data of AB grains, except that ^{26}Al/^{27}Al ratios of AB1 grains span a narrower range. The data are compared with predictions from supernova models that consider H ingestion into the He shell during the pre-supernova phase. In these models a mixture of explosive H and He burning occurs at the bottom of the He shell during passage of the supernova shock, forming the so-called O/nova zone. Mixing matter from the O/nova zone with matter from the overlying He/C zone and the stellar envelope shows that the isotopic compositions and trends of both AB1 and AB2 grains can be matched within the model uncertainties. This demonstrates that supernovae should be considered as potential sources of AB2 grains, in addition to J-type carbon stars and born-again asymptotic giant branch stars, as previously proposed.

Unified Astronomy Thesaurus concepts: Circumstellar matter (241); Meteorites (1038); Nucleosynthesis (1131); Supernovae (1668)

1. Introduction

Primitive solar system materials, e.g., undifferentiated meteorites, interplanetary dust particles, and cometary matter returned by NASA's Stardust mission, contain small quantities of so-called presolar grains that formed in the winds of evolved stars and in the ejecta of stellar explosions (Zinner 2014). These pristine dust grains can be analyzed in terrestrial laboratories for isotopic compositions and other physical properties. These laboratory studies have provided a wealth of astrophysical information, e.g., on stellar nucleosynthesis and evolution, mixing in supernova (SN) ejecta, dust formation in stellar environments, dust processing in the interstellar medium, and the inventory of stars that contributed dust to our solar system.

Identified stardust minerals include silicon carbide (SiC), graphite, silicon nitride, oxides (e.g., $MgAl_2O_4$ and Al_2O_3), and silicates. Most of these stardust grains were found in primitive meteorites because meteorites represent the most abundant type of extraterrestrial matter available for laboratory studies. Most abundant among the stardust minerals are silicates, which, however, were identified only 15 yr after the discovery of carbonaceous presolar grains (Messenger et al. 2003). The reason for this is that presolar silicates, in contrast to carbonaceous presolar grains, cannot be separated from primitive meteorites by chemical treatments and only the application of high-resolution ion-imaging techniques to thin sections of primitive solar system materials made their in situ discovery possible. Because in situ ion imaging is a time-consuming technique, much less information is available on the isotopic compositions of presolar silicates than for carbonaceous presolar grains.

Silicon carbide is the best-characterized presolar mineral. It was identified more than 30 yr ago (Bernatowicz et al. 1987) because it is tagged with noble gases of anomalous isotopic compositions (Lewis et al. 1994). Subsequently, it was found that the major elements C and Si, and numerous minor elements contained in presolar SiC, have highly anomalous isotopic compositions as well, the fingerprints of nucleosynthetic processes in their parent stars. Based on the isotopic compositions of C, N, and Si, SiC was divided into distinct populations (Zinner 2014). This includes the mainstream grains, which account for about 80%–90% of all grains (depending on grain size), and the minor types AB (originally defined as two distinct types A and B), C, X, Y, Z, and (putative) nova grains. The mainstream grains have ^{12}C/^{13}C ratios between 10 and 100 (solar: 89), and the ^{14}N/^{15}N ratios of most of them are higher than the solar ratio of 440, the ratio measured for the solar wind (Marty et al. 2011). In a plot of δ^{29}Si versus δ^{30}Si, the mainstream grains lie along a straight line defined by δ^{29}Si = 1.37 × δ^{30}Si–20 (Zinner et al. 2007), where δ^xSi = [(^{x}Si/^{28}Si)$_{\text{grain}}$/(^{x}Si/^{28}Si)$_{\text{solar}}$−1) × 1000, and x = 29 or 30, i.e., δ^xSi is the per mil deviation from the solar ^{x}Si/^{28}Si ratio. δ^{30}Si values of mainstream grains vary between about −50‰ and +150‰. The isotopic compositions of heavy elements show the signatures of slow neutron-capture nucleosynthesis (s-process, Käppeler et al. 2011), which points toward low-mass (1.5–3 $M_\odot$) asymptotic giant branch (AGB) stars of about solar or supersolar metallicity as parent stars (e.g., Lugaro et al. 2018, and references therein). The minor type Y and Z grains (a few % of all SiC grains, depending on grain size), which fall to the ^{30}Si-rich side of the Si mainstream line, were also proposed to originate from low-mass AGB stars, but with metallicities lower than solar (Hoppe et al. 1997; Amari et al. 2001b). This low-metallicity scenario, however,

---

[6] NuGrid Collaboration, http://www.nugridstars.org.

was recently questioned (Liu et al. 2019). The type C (∼0.1% of all SiC grains) and X grains (∼1% of all SiC grains) are believed to originate from core-collapse supernovae (CCSNe; Amari et al. 1992; Hoppe et al. 1996b; Nittler et al. 1996; Gyngard et al. 2010). These grains show strong depletions (X grains) or enrichments (C grains) in the heavy Si isotopes. Their $^{12}C/^{13}C$ ratios span a large range from <10 to >10,000; other characteristic features of X and C grains are enrichments in ^{15}N and high initial $^{26}Al/^{27}Al$ ratios of typically >0.1. Putative nova grains (∼0.1% of all SiC grains) have low $^{12}C/^{13}C$ ratios of <10, low $^{14}N/^{15}N$ ratios of <40, and high initial $^{26}Al/^{27}Al$ ratios of up to 0.2 (Amari et al. 2001a); their origins in the outflows of nova explosions, however, were questioned and SNe were proposed for at least some of the putative nova grains instead (Nittler & Hoppe 2005; Pignatari et al. 2015; Liu et al. 2017a; Hoppe et al. 2018b).

The type AB grains constitute a few percent of all SiC grains. AB grains have $^{12}C/^{13}C \lesssim 10$, a large range of $^{14}N/^{15}N$ ratios from ∼30 to 10,000, Si-isotopic compositions along the Si mainstream line, and higher initial $^{26}Al/^{27}Al$ ratios than the mainstream grains (Zinner 2014). AB grains were subdivided into two subtypes depending on the N-isotopic ratio. AB grains with isotopically heavy N ($^{14}N/^{15}N$ < 440 = solar) have been named AB1, and those with light N ($^{14}N/^{15}N \geqslant 440$) are called AB2 (Liu et al. 2017a). The origin of AB grains is still a matter of debate. Proposed major stellar sources include born-again AGB stars (Amari et al. 2001b) and J-type carbon stars (Liu et al. 2017b) for AB2 grains, and SNe for AB1 grains (Liu et al. 2017a). Several theoretical models are available today for SNe and AGB stars, and while several uncertainties still remain, nucleosynthesis results can be analyzed and compared with observations. On the other hand, from an evolutionary point of view, J-type C stars are still somewhat of a mystery: We do not know how they form, nor what they evolve into. Recent population synthesis modeling by Sengupta et al. (2013) suggested these stars formed in nova systems where the companion accreted nova ejecta, and subsequently merged with the white dwarf. However, little is known about the nucleosynthetic signatures of these events. Sengupta et al. (2013) explored the possibility that J-type carbon stars could evolve to an AGB-like phase, where they would eject material in a similar way to normal AGB stars. If their initial mass and metallicity would allow these stars to avoid third dredge-up, they could conceivably produce dust grains in a similar manner to AGB stars, but with AB grain-like compositions. However, if third dredge-up does happen, the composition would likely become similar to those of normal AGB stars because of high ^{12}C production. Therefore it is still unclear if J-type C stars can condense AB SiC grains at all, making this scenario highly speculative, and with no comprehensive nucleosynthesis calculations to compare it with.

Here, we report on high spatial resolution measurements of C-, N-, Mg–Al-, Si-, and S-isotopic compositions of 38 submicrometer-sized AB grains from the Murchison CM2 meteorite by NanoSIMS ion imaging. Particular care was used to exclude contamination on or around grains and measurements of grain aggregates (containing two or more SiC grains), as this can seriously affect the interpretation of the isotope data of AB grains. The main goal of our study is to explore whether SNe could account for the isotopic signatures of both AB1 and AB2 grains. This would provide an alternative or complementary scenario to J-Type C stars being the dominant sources of AB2 grains, as proposed by Liu et al. (2017b). For this purpose, we compare the isotope data of AB grains with predictions from SN models of Pignatari et al. (2015), who consider H ingestion into the He shell during the pre-SN phase. Except for one specific grain, we do not try to find exact matches for the isotopic compositions of individual AB grains by specific SN mixtures, but rather explore whether the trends and ranges seen in the isotope data of AB grains can be reproduced. Preliminary data of this work were published in two conference proceedings (Hoppe et al. 2019a, 2019b).

2. Experimental

Hundreds of SiC grains from the Murchison separate KJD (median size: 0.81 μm; Amari et al. 1994), dispersed on a clean gold foil, were screened by C and Si ion-imaging with the NanoSIMS ion probe at the Max Planck Institute for Chemistry. For this purpose, a focused Cs^+ primary ion beam (∼1 pA, 100 nm) was rastered over 136 $30 \times 30\ \mu m^2$ sized areas on the gold foil and negative secondary ion images of ^{12}C, ^{13}C, ^{28}Si, ^{29}Si, and ^{30}Si were recorded in multi-collection (256×256 pixels, 15,000 μs/pixel). Visual inspection of ion images identified 38 AB grains, based on their large ^{13}C enrichments. Follow-up measurements with high spatial resolution and a raster only slightly larger than the grain sizes of C, N (measured as CN), Mg–Al, Si, and S isotopes were conducted in three sessions: (i) Measurement of C and Si isotopes with the same detector setup as described above on 38 AB grains, employing the Cs^+ primary ion source (∼1 pA, 100 nm, raster 1.5×1.5–$4 \times 4\ \mu m^2$). (ii) Measurement of negative secondary ions of $^{12}C^{14}N$, $^{12}C^{15}N$, ^{28}Si or ^{29}Si, ^{32}S, and ^{34}S on 37 AB grains, employing the Cs^+ primary ion source (∼1 pA, 100 nm, raster raster 1.5×1.5–$3 \times 3\ \mu m^2$). (iii) Measurement of positive secondary ions of ^{24}Mg, ^{25}Mg, ^{26}Mg, ^{27}Al, and ^{28}Si on 34 AB grains, employing the recently installed high-resolution Hyperion O^- primary ion source (∼3 pA, 100 nm, raster 1.5×1.5–$3 \times 3\ \mu m^2$; see Hoppe et al. 2018a; Nittler et al. 2018). The relative Al^+/Mg^+ sensitivity factor (1.56), required to calculate initial $^{26}Al/^{27}Al$ ratios, was taken from Hoppe et al. (2010).

Ion images of ^{12}C, $^{13}C/^{12}C$, and ^{27}Al along with the SEM image of SiC grain KJD-102 are displayed in Figure 1. The C-isotopic ratio image illustrates the importance of high spatial resolution measurements, as the object seen in the SEM image apparently is composed of two distinct SiC grains: one AB grain with its characteristic high ^{13}C enrichment, and in this case, also high Al concentration; and another SiC grain with a lower $^{13}C/^{12}C$ ratio and low Al concentration. Without a sufficient resolution of these two grains, their combined ion signals would still show the characteristic C-isotopic ratio of AB grains ($^{12}C/^{13}C$ < 10), but the isotopic signatures of the AB grain would be distorted and interpretations misled.

3. Results

Carbon-, N-, Al-, Si-, and S-isotopic compositions of the 38 AB grains from this study are presented in Table 1 and in Figures 2–4. Except for one outlier, grain KJD-134b, which has $^{12}C/^{13}C$ = 15.6 and $^{14}N/^{15}N$ = 36, $^{12}C/^{13}C$ ratios are between 1.6 and 10 and $^{14}N/^{15}N$ ratios between 50 and 10,000,

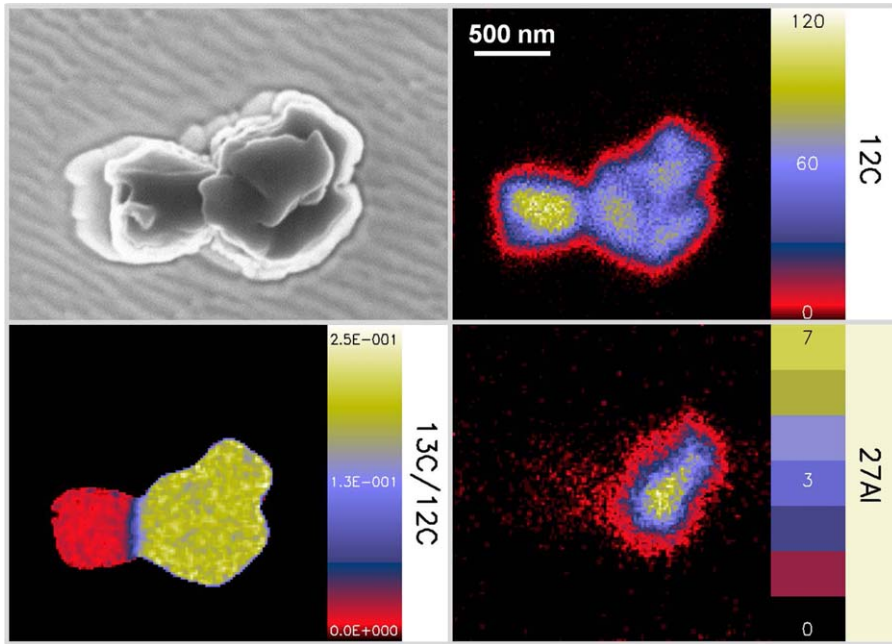**Figure 1.** SEM image and NanoSIMS ion images of $^{12}C^-$, $^{13}C^-/^{12}C^-$, and $^{27}Al^+$ of the presolar SiC AB grain KJD-102. The scale bar shown in the $^{12}C^-$ image applies to all images. From the $^{13}C^-/^{12}C^-$ image it can be seen that the object in the SEM image consists of two distinct SiC grains and that only the right part is an SiC grain of type AB.

falling well within the ranges of previously studied AB grains (Figure 2). Seventeen of the grains are of type AB1 (including KJD-134b), and 20 of type AB2; for one grain (KJD-101) we lack N isotope data, i.e., it cannot be assigned to one of the AB subtypes. In Figure 2 grain KJD-134b plots in the area occupied by putative nova and SN grains. While its $^{26}Al/^{27}Al$ ratio (0.13, which is the highest value among our studied AB grains) is also compatible with those of putative nova or SN grains, its Si-isotopic composition is that of AB grains, which makes a clear assignment to one of the grain groups impossible. As we do not wish to define a new subtype for grain KJD-134b, we assign it here to subtype AB1. In most cases, Mg was found to be dominated by ^{26}Mg, which is clear evidence for ^{26}Al decay (half-life 716,000 yr). Inferred initial $^{26}Al/^{27}Al$ ratios are between 10^{-4} and 0.13. There is a rough negative correlation between $^{26}Al/^{27}Al$ and $^{14}N/^{15}N$ for AB1 grains (Figure 3). Some of the AB2 grains follow this trend, but overall, AB2 grains exhibit a larger scatter in the $^{26}Al/^{27}Al$ versus $^{14}N/^{15}N$ representation. Silicon-isotopic compositions plot along the Si mainstream line, with $\delta^{29}Si$ values between $-80‰$ and $+230‰$, and $\delta^{30}Si$ values between $-50‰$ and $+160‰$ (Figure 4). There is no clear distinction between the Si-isotopic compositions of AB1 and AB2 grains. Weighted linear regressions according to York-Mahon (Mahon 1996; York 1969) give $\delta^{29}Si = (1.43 \pm 0.16) \times \delta^{30}Si - (14 \pm 11)$ for AB1 grains and $(1.66 \pm 0.32) \times \delta^{30}Si - (19 \pm 16)$ for AB2 grains (the reduced chi square values of 1.12 and 3.2, respectively, for the fits are included in the errors), i.e., the slopes and intercepts are fully compatible with the Si mainstream line. The $^{34}S/^{32}S$ ratios of all AB grains are normal within $\sim2\sigma$; The 13 AB2 grains with S/Si < 0.01 have on average $\delta^{34}S = -43 \pm 31‰$ and 11 out of the 13 grains have $\delta^{34}S < 0$. The 10 AB1 grains with S/Si < 0.01 have on average $\delta^{34}S = 1 \pm 44‰$ and 5 out of the 10 grains have $\delta^{34}S < 0$.

4. Discussion

4.1. Comparison with Isotope Data of AB Grains from Previous Studies

In the literature, simultaneous C, N, Mg–Al, and Si isotope data exist for 88 AB grains (Hoppe et al. 1994, 2010; Huss et al. 1997; Amari et al. 2001b; Liu et al. 2017b), i.e., our data set, comprising 34 AB grains with C, N, Mg–Al, and Si isotope data, has increased this number by almost 40%. A comparison of our new isotope data for AB1 and AB2 grains with those previously obtained shows good agreement in general (Figures 2 and 4), except for the combined $^{26}Al/^{27}Al$ and $^{14}N/^{15}N$ data of AB1 grains (Figure 3). For the latter, many of the $^{26}Al/^{27}Al$ ratios from previous studies are lower than the new data presented here. This cannot be explained by different Al^+/Mg^+ sensitivity factors inferred in the different SIMS studies, but points toward a higher level of unrecognized Al contamination in part of the previous data, as discussed by Groopman et al. (2015).

4.2. AB Grains in the Context of J-type C Stars and Born-again AGB Stars

Liu et al. (2017b) have favored J-type C stars as dominant sources of AB2 grains based on observed C- and N-isotopic compositions and missing s-process signatures. J-type C stars have $^{12}C/^{13}C$ ratios between ~2 and 12 (Ohnaka & Tsuji 1999) and $^{14}N/^{15}N$ ratios between 900 and 3200 (Hedrosa et al. 2013), as inferred from spectroscopic observations, and in agreement with AB2 grains. This makes J-type C stars plausible sources of AB2 grains. However, as we pointed out in the Introduction section, we do not know much about these objects, and there are no nucleosynthesis yields from these objects to compare with measurements on presolar grains, which makes a final judgment difficult.

Table 1
Carbon-, N-, Si-, and S-isotopic Compositions and Inferred ^{26}Al/^{27}Al Ratios of Presolar SiC AB Grains from Murchison Separate KJD

Grain	Type	^{12}C/^{13}C	^{14}N/^{15}N	^{26}Al/^{27}Al (10^{-3})	δ^{29}Si (‰)	δ^{30}Si (‰)	δ^{34}S (‰)
KJD-101	AB	4.34 ± 0.06			141 ± 37	114 ± 45	
KJD-102	AB2	5.82 ± 0.02	552 ± 42	10.6 ± 1.4	121 ± 5	87 ± 6	26 ± 25
KJD-103	AB2	3.94 ± 0.01	3750 ± 400	2.4 ± 0.2	69 ± 6	44 ± 7	21 ± 61
KJD-105	AB2	5.97 ± 0.02	769 ± 157		5 ± 6	22 ± 8	−34 ± 82
KJD-108a	AB1	2.60 ± 0.01	122 ± 9	3.5 ± 1.0	71 ± 10	64 ± 12	164 ± 254
KJD-108b	AB2	8.63 ± 0.07	1217 ± 279	<0.56	10 ± 11	40 ± 13	−229 ± 261
KJD-111	AB2	9.88 ± 0.09	819 ± 71	<0.48	81 ± 13	74 ± 16	−32 ± 165
KJD-116	AB1	3.93 ± 0.03	74 ± 2	22.6 ± 1.7	−34 ± 23	3 ± 29	34 ± 73
KJD-119	AB2	2.49 ± 0.01	523 ± 59		−47 ± 16	6 ± 20	20 ± 90
KJD-121	AB1	8.01 ± 0.07	353 ± 49	<3.9	59 ± 14	53 ± 17	205 ± 189
KJD-123	AB2	8.88 ± 0.05	964 ± 201	5.2 ± 0.9	84 ± 9	5 ± 11	−60 ± 114
KJD-134a	AB2	6.33 ± 0.14	3254 ± 679	5.5 ± 0.4	29 ± 44	69 ± 54	−5 ± 58
KJD-134b	AB1	15.57 ± 0.84	36 ± 2	127.7 ± 4.3	−2 ± 74	−41 ± 89	16 ± 111
KJD-135	AB1	1.94 ± 0.01	89 ± 4	9.2 ± 1.5	66 ± 10	26 ± 12	13 ± 44
KJD-136	AB2	8.74 ± 0.08	1640 ± 328	0.36 ± 0.1	34 ± 14	27 ± 18	−74 ± 111
KJD-139	AB2	9.30 ± 0.06	1325 ± 322	2.4 ± 1.0	43 ± 9	28 ± 11	−417 ± 171
KJD-141	AB2	4.59 ± 0.03	5263 ± 890	<9.7	−25 ± 12	46 ± 16	43 ± 58
KJD-148	AB2	6.39 ± 0.03	9552 ± 2881	0.6 ± 0.1	19 ± 6	53 ± 8	−188 ± 129
KJD-154	AB1	4.20 ± 0.02	347 ± 54	1.6 ± 0.5	178 ± 13	135 ± 16	−34 ± 197
KJD-174	AB1	2.48 ± 0.03	51 ± 4	21.5 ± 6.0	−22 ± 35	96 ± 45	54 ± 154
KJD-176	AB1	2.44 ± 0.02	123 ± 34		−50 ± 27	−17 ± 34	809 ± 626
KJD-17a	AB1	3.19 ± 0.01	171 ± 6	9.7 ± 0.5	72 ± 9	62 ± 10	52 ± 82
KJD-17b	AB1	4.16 ± 0.05	221 ± 14	8.5 ± 1.1	−16 ± 29	34 ± 37	115 ± 71
KJD-180	AB1	3.09 ± 0.01	84 ± 2	5.4 ± 0.3	82 ± 9	79 ± 11	−8 ± 78
KJD-181	AB2	4.82 ± 0.02	1787 ± 565	11.7 ± 4.1	−47 ± 11	−53 ± 13	−245 ± 123
KJD-183	AB2	5.38 ± 0.03	817 ± 366	2.9 ± 2.1	128 ± 12	91 ± 14	−15 ± 155
KJD-22	AB2	9.92 ± 0.10	740 ± 112	6.1 ± 0.8	127 ± 15	107 ± 18	226 ± 109
KJD-23	AB1	3.05 ± 0.01	116 ± 5	8.5 ± 0.8	−2 ± 9	2 ± 11	−108 ± 107
KJD-27	AB2	5.16 ± 0.04	958 ± 114	2.7 ± 0.3	−3 ± 17	−31 ± 21	120 ± 56
KJD-30	AB2	4.21 ± 0.02	833 ± 85	6.0 ± 0.5	49 ± 12	39 ± 15	−93 ± 85
KJD-32	AB1	4.13 ± 0.05	310 ± 21	6.9 ± 0.8	225 ± 24	146 ± 28	−7 ± 153
KJD-33	AB1	4.32 ± 0.04	82 ± 5	12.0 ± 1.3	−78 ± 16	−34 ± 20	−73 ± 85
KJD-35	AB1	6.47 ± 0.04	288 ± 14	1.9 ± 0.2	60 ± 11	29 ± 13	−202 ± 127
KJD-41	AB2	3.54 ± 0.03	598 ± 50	9.4 ± 0.6	47 ± 17	52 ± 20	−114 ± 144
KJD-45	AB1	2.49 ± 0.01	53 ± 1	27.6 ± 0.8	35 ± 17	76 ± 21	−14 ± 115
KJD-49	AB2	6.28 ± 0.03	1535 ± 160	<0.15	17 ± 10	7 ± 12	−10 ± 110
KJD-54	AB2	5.60 ± 0.06	525 ± 58	<0.51	53 ± 21	16 ± 25	−9 ± 28
KJD-8	AB1	4.00 ± 0.03	329 ± 31	3.9 ± 0.7	200 ± 15	162 ± 18	193 ± 171
Solar		89	441		0	0	0

Note. Errors are 1σ. Upper limits of ^{26}Al/^{27}Al are given when 1σ errors are larger than 50% and are based on 2σ errors. δ^iX = [$(^iX/^jX)_{grain}/(^iX/^jX)_{std}$−1] × 1000; ^{j}X = ^{28}Si or ^{32}S and $(^{29}Si/^{28}Si)_{std}$ = 0.050804, $(^{30}Si/^{28}Si)_{std}$ = 0.033532, and $(^{34}S/^{32}S)_{std}$ = 0.0441626.

Early R-type C stars and CO novae have been considered as potential sources of AB2 grains as well, but Liu et al. (2017b) pointed out that their low abundances make significant contributions to the AB2 grain population unlikely. Born-again AGB stars, which are stars that have experienced either a late or very late thermal pulse and subsequently returned to the AGB (see Herwig 2005 for a review), were excluded by Liu et al. (2017b) as a dominant source of AB2 grains because 11 out of the 12 studied AB2 grains showed about normal (solar) isotopic compositions of heavy elements, which is incompatible with the predicted large isotopic anomalies from the s-process or intermediate neutron-capture nucleosynthesis (i-process, Herwig et al. 2011) that would be expected in dust from such stars. While the born-again AGB star Sakurai's object showed i-process signatures (Herwig et al. 2011), it cannot be excluded that other H-ingestion events in post-AGB stars would not activate the i-process. Indeed, H-ingestion events could cause the He intershell region to become quickly

unstable, following global violent oscillations (Herwig et al. 2014), before the ^{13}C neutron source has enough time to produce heavy elements. Furthermore, in case of a low-mass star progenitor with mass lower than 1.5 $M_\odot$, the s-process enrichment from the previous AGB evolution would also have been extremely mild and difficult to measure. Therefore, we point out that post-AGB stars should not be completely ruled out as potential sources of at least some AB2 grains without neutron-capture nucleosynthesis signatures.

4.3. AB Grains in the Context of Supernova Models

Low ^{12}C/^{13}C ratios are the signature of hydrostatic and explosive hydrogen burning (e.g., Jose & Hernanz 1998; Rauscher et al. 2002; Wiescher et al. 2010, and references therein). While explosive H burning produces much ^{15}N, i.e., low ^{14}N/^{15}N ratios, hydrostatic H burning results in high ^{14}N/^{15}N ratios. Explosive H burning occurs in novae and SNe, which were considered as potential stellar sources for presolar
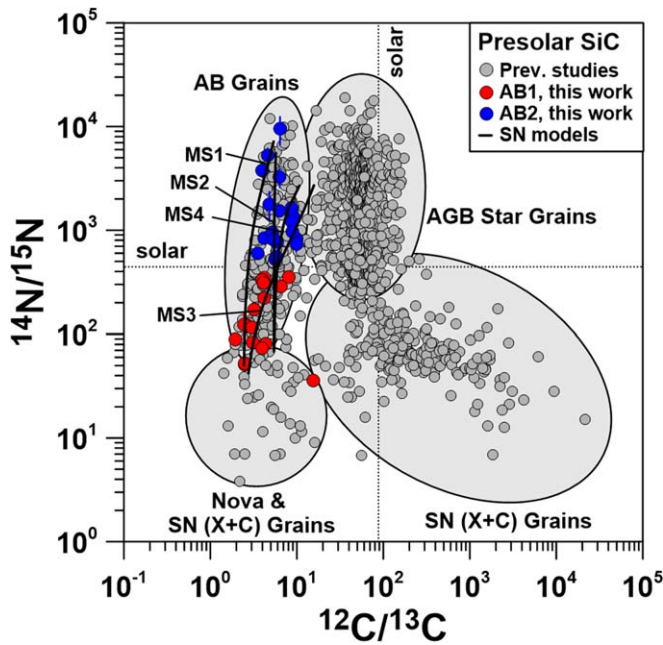
Figure 2. Carbon- and N-isotopic compositions of 37 SiC AB grains from Murchison separate KJD. AB1 grains ($^{14}N/^{15}N < 440$) are shown in red and AB2 grains ($^{14}N/^{15}N \geqslant 440$) in blue. Errors are 1σ. Selected literature data of SiC grains from all SiC populations (Hoppe et al. 1994, 1996a, 2000, 2010; Nittler 1996; Huss et al. 1997; Amari et al. 2001a, 2001b; Lin et al. 2002; Besmehn & Hoppe 2003; Nittler & Hoppe 2005; Marhas et al. 2008; Xu et al. 2015; Liu et al. 2016, 2017a, 2017b, 2018) are given in gray for comparison. The solar system isotopic compositions are shown by dashed lines. Predictions for four SN mixing models are shown as black solid lines. These models consider mixing of matter from the O/nova and He/C zones in SN models 25T-H and 25T-H10 (Pignatari et al. 2015) with matter from the envelopes in models 25T-H and 25T-H10 (models MS1 and MS2), or alternatively, with matter from the envelope of a 15 $M_\odot$ SN (Pignatari et al. 2013; models MS3 and MS4).

Figure 3. The $^{26}Al/^{27}Al$ and $^{14}N/^{15}N$ ratios of 28 SiC AB grains from Murchison separate KJD with relative 1σ errors for $^{26}Al/^{27}Al$ ratios smaller than 50%. AB1 grains ($^{14}N/^{15}N < 440$) are shown in red and AB2 grains ($^{14}N/^{15}N \geqslant 440$) in blue. Errors are 1σ. Literature data of SiC AB grains (Hoppe et al. 1994, 2010; Huss et al. 1997; Amari et al. 2001b; Liu et al. 2017a) are given in gray for comparison. The solar system $^{14}N/^{15}N$ ratio is shown by the dashed line. Predictions for the four SN mixing models from Figure 2 (models MS1-4), and in addition a mixing model that considers matter from the O/nova and He/C zones in SN model 25T-H20 (Pignatari et al. 2015) and matter from the envelope of a 15 $M_\odot$ SN (Pignatari et al. 2013; model MS5), are shown as black lines. Solid lines represent mixtures with C/O $\geqslant$ 1 and dotted lines those with C/O < 1.

SiC grains with enhanced (relative to solar) ^{15}N abundances, namely, putative nova grains (Amari et al. 2001a), the X and C grains (e.g., Amari et al. 1992; Nittler et al. 1996; Hoppe et al. 2000, 2010; Lin et al. 2010; Pignatari et al. 2013, 2015; Xu et al. 2015; Gyngard et al. 2018), and about half of the AB grains, namely, subtype AB1 (Liu et al. 2016, 2017a). It was pointed out by Liu et al. (2017a) that novae are unlikely sources of AB1 grains and that AB1 grains most likely formed in the ejecta of SN explosions.

Here, we explore whether AB grains with isotopically light nitrogen, i.e., those of subtype AB2, which have $^{14}N/^{15}N \geqslant 440$, could originate from SNe as well. We compare our results for AB grains, along with those from the literature, with SN model predictions by Pignatari et al. (2015), which have previously been used to account for the isotope data of AB1, C, and X grains (Liu et al. 2017a; Hoppe et al. 2018b).

Pignatari et al. (2015) provide isotope data for a set of 25 $M_\odot$ CCSNe of solar metallicity that experienced H ingestion into the He shell prior to the explosion. During the final stages of the massive star progenitor, the energy generation at the bottom of the convective He-burning shell becomes progressively unstable until convection is switched off. In the meantime, H starts to be ingested from more external layers into regions where the convective He shell was located. In the model, the convective He shell does not reignite before the CCSN explosion, leaving a trace of H in the He shell, together with significant ^{13}C and ^{14}N enrichments (Pignatari et al. 2015).
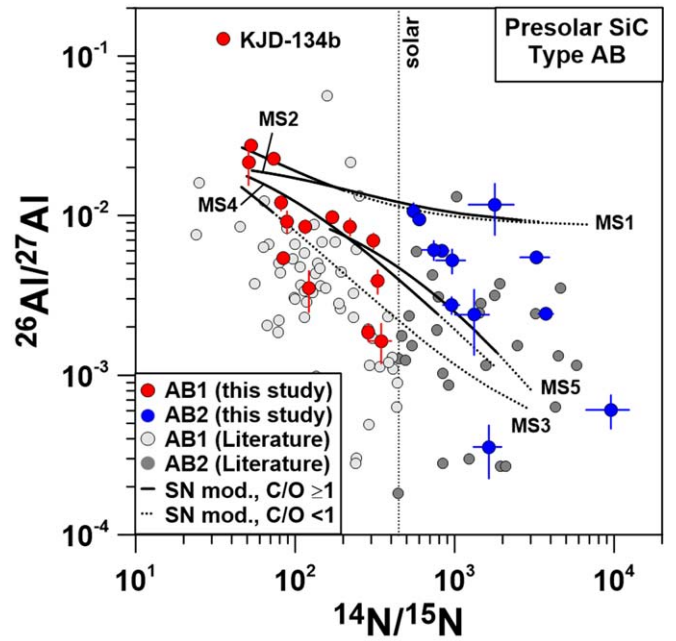
Supernova models considered in this work are 25T-H, 25T-H10, and 25T-H20, according to the naming scheme used by Pignatari et al. (2015). Model 25T-H considers 1.2% H left in the He shell layers, consistent with the original 25 $M_\odot$ progenitor (Pignatari et al. 2016). In models 25T-Hx, hydrogen concentrations are reduced by a factor of x, i.e., models 25T-H10 and 25T-H20 consider 0.12% and 0.06% of H in the He shell. Compared to the original 25 $M_\odot$ stellar simulations, these models use artificially increased temperature and density in the He shell to mimic the temperature and density evolution of a 15 $M_\odot$ SN during the SN explosion (see discussion in Pignatari et al. 2015 for details).

Explosive H burning occurs at the bottom of the He shell during passage of the SN shock, together with explosive He burning. This leads to unique elemental and isotopic patterns. In these models, He shell ejecta can be classified into three distinct zones: At the bottom, a thin (<0.04 $M_\odot$) C/Si zone, and above the O/nova and He/C zones. In contrast to the underlying and overlying Si/C and He/C zones, the O/nova zone has C/O < 1. Most of the O/nova zone and the bottom of the He/C zone exhibit low $^{12}C/^{13}C$, $^{14}N/^{15}N$, and high $^{26}Al/^{27}Al$ ratios, a signature typical of nova nucleosynthesis (e.g., José & Hernanz 2007; Denissenkov et al. 2014; Figure 5). The O/nova zone extends from 6.82 to 7.16 $M_\odot$ (25T-H) and from 6.85 to 7.00 $M_\odot$ (25T-H10, 25T-H20). Its size would typically decrease with increasing mass of the massive star progenitor, increase with increasing energy of the SN explosion, and increase with increasing amount of H that is left from the pre-SN H-ingestion event. The amount of H that is
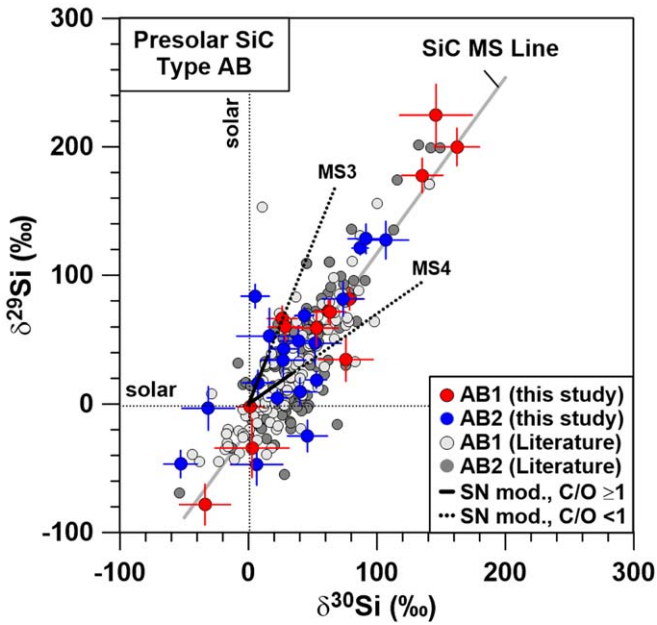
Figure 4. Silicon-isotopic compositions of 32 SiC AB grains from Murchison separate KJD with 1σ errors in δ^{30}Si smaller than 30‰. AB1 grains (^{14}N/^{15}N < 440) are shown in red and AB2 grains (^{14}N/^{15}N ⩾ 440) in blue. Errors are 1σ. Literature data of SiC AB grains (Hoppe et al. 1994, 1996a, 2010; Huss et al. 1997; Amari et al. 2001b; Lin et al. 2002; Marhas et al. 2008; Liu et al. 2017a, 2017b, 2018) are given in gray for comparison. The solar system Si-isotopic composition is shown by the dashed lines. Predictions for the two SN mixing models from Figure 2 with the envelope composition of a 15 $M_\odot$ SN (Pignatari et al. 2013; models MS 3 and MS4) are shown as black lines. Mixtures with ^{14}N/^{15}N > 100 are shown as dotted lines and those having ^{14}N/^{15}N > 440 as solid lines.

Figure 5. Profiles of ^{12}C/^{13}C, ^{14}N/^{15}N, and ^{26}Al/^{27}Al ratios in the interior of a 25 $M_\odot$ SN according to models 25T-H and 25T-H10 of Pignatari et al. (2015). The yellow and blue areas denote the He/C and O/nova zones, respectively. The O/nova zone has experienced explosive H burning and shows local enrichments in ^{13}C, ^{15}N, and ^{26}Al.

ingested in the He shell is extremely uncertain because the massive star progenitor is based on a one-dimensional model, while H-ingestion events require multi-dimensional hydrodynamic simulations (e.g., Stancliffe et al. 2011; Herwig et al. 2014; Woodward et al. 2015). We therefore consider SN models with a factor of 20 as a range of H enrichment. Finally, the overlying He/C zone, which extends to 9.23 $M_\odot$, still carries milder explosive H-burning signatures within a C-rich region at the bottom.

We examine five different mixing scenarios to compare them directly with the isotopic compositions of AB1 and AB2 grains (Table 2). In each, we mix material from the combined O/nova and He/C zones with material in the stellar envelope in varying proportions. Scenarios MS1 and MS2 use the 25T-H and 25T-H10 models, respectively. For scenarios MS3 and MS4, we use the O/nova and He/C zone material from the same two models, but take the envelope composition from the 15 $M_\odot$ SN model 15r of Pignatari et al. (2013), which is based on the same stellar code, to mimic the envelope compositions of lower mass SNe. Lower mass SNe have lower ^{14}N/^{15}N and ^{26}Al/^{27}Al ratios in their envelopes than the more massive SNe, which gives better fits to many of the combined N- and Al-isotope data (see below). In scenario MS5, we take the interior composition from model 25T-H20, and the envelope composition from model 15r. Carbon-, N-, and Al-isotopic compositions of the combined O/nova and He/C zones and of the envelope for the five mixing scenarios are given in Table 2. The SN model predictions shown in Figures 2 and 3 consider correction factors of 3 for ^{12}C/^{13}C and 5 for ^{26}Al/^{27}Al for the
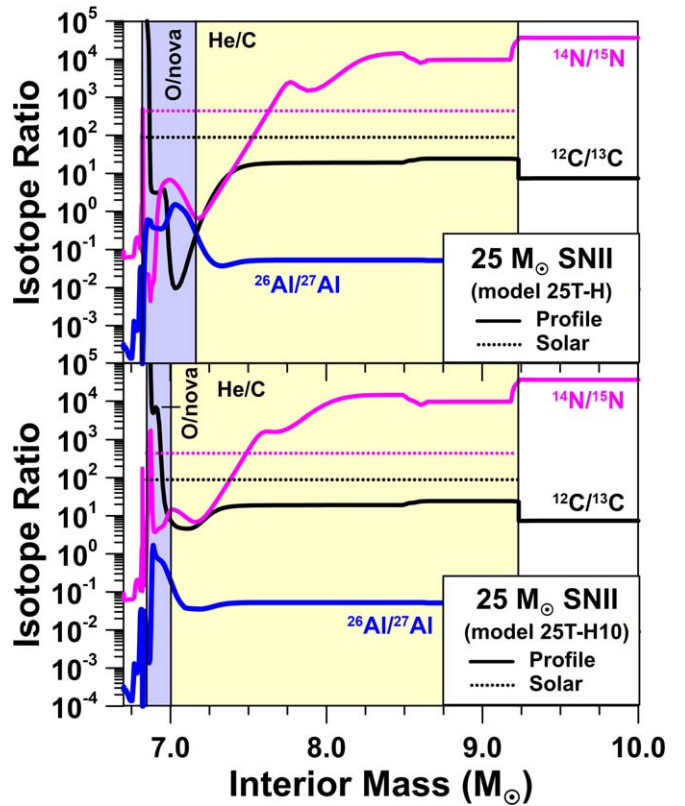
combined O/nova and He/C zone compositions (see Table 2 and below).

The C and N data of both AB1 and AB2 grains are well reproduced by our mixing models if the ^{12}C/^{13}C ratio in the combined O/nova and He/C zones is reduced by a factor of 3, which is within present model uncertainties. Indeed, the ^{13}C abundance is strongly affected by how the H ingestion forms and develops, and by the following SN explosion energy. For instance, the ^{12}C/^{13}C ratio of the O/nova zone in model 25T-H (0.083) is about a factor of 400 lower than that of model 25T-H10 (35.4), while the ^{14}N/^{15}N ratio varies much less (3.5 versus 5.9; Figure 5), demonstrating how sensitive the ^{12}C/^{13}C ratio is to (local) variations in H concentration. Furthermore, the amount of ^{13}C made by H-ingestion, before the SN explosion, depends on several details of the event, such as the amount of H and the speed with which H is ingested. Multidimensional hydrodynamics models for H ingestion in massive stars at solar-like metallicity are required to provide this information and the respective stellar structure response. Models are already available for ingestion of H into the He shell in AGB stars, post-AGB stars, and in rapidly accreting white dwarfs (e.g., Stancliffe et al. 2011; Herwig et al. 2014; Denissenkov et al. 2019). On the other hand, the first hydrodynamics simulations are only becoming available now for H-ingestion in massive stars, and only at zero metallicity (Clarkson et al. 2018). Therefore, our results will be extremely important to constrain the next generation of H ingestion and SN explosion models. The models also reproduce the weak positive correlation between ^{12}C/^{13}C and ^{14}N/^{15}N seen in the

Table 2
Supernova Mixing Scenarios and Their End Member Compositions

Mixing Scenario	MS1	MS2	MS3	MS4	MS5
Model O/nova+HeC	25T-H	25T-H10	25T-H	25T-H10	25T-H20
Model Envelope	25T-H	25T-H10	15r	15r	15r
^{12}C/^{13}C$_{int}$[a]	7.3	16.3	7.3	16.3	18.9
^{12}C/^{13}C$_{int}$/3[b]	2.4	5.4	2.4	5.4	6.3
^{12}C/^{13}C$_{env}$[c]	7.6	7.6	18.9	18.9	18.9
^{14}N/^{15}N$_{int}$[a]	5.2	35	5.2	35	119
^{14}N/^{15}N$_{env}$[c]	36100	36100	4270	4270	4270
^{26}Al/^{27}Al$_{int}$[a]	0.25	0.10	0.25	0.10	0.047
^{26}Al/^{27}Al$_{int}$/5[d]	0.05	0.02	0.05	0.02	9.4×10^{-3}
^{26}Al/^{27}Al$_{env}$[c]	8.6×10^{-3}	8.6×10^{-3}	5.2×10^{-4}	5.2×10^{-4}	5.2×10^{-4}

Notes.
[a] Composition of combined O/nova and He/C zones.
[b] Used in Figure 2.
[c] Envelope composition.
[d] Used in Figure 3.

data of AB grains (Figure 2). AB1 grain KJD-134b, which has the highest ^{12}C/^{13}C and lowest ^{14}N/^{15}N of the grains presented here, does not follow this trend, which we discuss below. Our mixing models can also account for the combined ^{26}Al/^{27}Al and ^{14}N/^{15}N data of most AB grains if the ^{26}Al/^{27}Al ratio from the combined O/nova and He/C zones is decreased by a factor of 5. The ^{26}Al/^{27}Al ratio depends sensitively on the interplay of ^{26}Al production by ^{25}Mg(p,γ)^{26}Al and destruction of ^{26}Al by neutron captures at temperatures $>3 \times 10^8$ K. This leads to relatively large uncertainties on ^{26}Al/^{27}Al in the O/ nova zone when one-dimensional models are considered and the factor of 5 lower ^{26}Al/^{27}Al than predicted by models 25T-Hx appears conceivable. As for ^{13}C, the amount of ^{26}Al made during the H-ingestion event is also still quite uncertain. Again, while the combined H-burning and He-burning nucleosynthesis in pre-supernova and explosive conditions is an anomalous feature measured in presolar grains that can be captured from the one-dimensional models used in this work, these results will be important for the next generation of three-dimensional H ingestion and SN explosion models. The mixing models predict a negative correlation between ^{26}Al/^{27}Al and ^{14}N/^{15}N, with a larger scatter in ^{26}Al/^{27}Al for higher ^{14}N/^{15}N if SNe with a range of masses are considered. Most of our AB grain data are encased by mixing models SM1-5 (Figure 3). The lower bound of these models in Figure 3, defined by mixing model SM3, would be shifted to lower ^{26}Al/^{27}Al ratios if we were to also consider the envelope composition from the 12 $M_\odot$ SN model of Woosley & Heger (2007), which has ^{14}N/^{15}N = 2610 and ^{26}Al/^{27}Al = 4.4×10^{-4}; with this, only AB1 grain KJD-134b and AB2 grain KJD-148, which has the highest ^{14}N/^{15}N ratio, would not be covered by our mixing models. The moderate negative correlation between ^{26}Al/^{27}Al and ^{14}N/^{15}N for AB1 grains, which was similarly observed by Liu et al. (2017a), is in line with our SN mixing model predictions.

The C, N, and Al isotope data of grain KJD-134b are compatible with those of X and C grains and are well reproduced by mixing sublayers from the O/nova zone alone in model 25T-H10 and by considering a C-N fractionation during SiC condensation of a factor of 50 (see Hoppe et al. 2018b). C-N fractionation increases the ^{14}N/^{15}N ratio considerably because of high concentrations of radioactive ^{14}C (half-life

5700 yr) in the specific mixture to match the isotope data of grain KJD-134b. Note that ^{14}C concentrations are comparatively low when matter from the whole O/nova and He/C zones is mixed with matter from the envelope, so that in mixing scenarios, MS1-5 ^{14}N/^{15}N ratios would be only slightly affected by C-N fractionation, which was therefore ignored.

Our mixing models predict only comparatively small Si isotope anomalies. Silicon isotope anomalies are generally smaller for a lower progenitor mass for the same N-isotopic ratio. For supersolar ^{14}N/^{15}N ratios (i.e., AB2 grains), ^{29}Si and ^{30}Si are typically enriched by a few percent. For mixtures having N-isotopic compositions of AB1 grains, enrichments in ^{29}Si and ^{30}Si are larger, but the magnitude of predicted Si isotope anomalies is still small compared with those of typical SN X and C grains. This is qualitatively consistent with the Si-isotopic compositions of AB grains, which plot along the Si mainstream line (Figure 4). Median δ^{29}Si and δ^{30}Si values of our AB grains grains with errors in δ^{30}Si of less than 30‰ are 59‰ and 53‰ (AB1), and 47‰ and 39‰ (AB2), respectively, which is slightly higher than the values of 33‰ and 39‰ of mainstream grains from the literature (Hynes & Gyngard 2009).

Given the uncertainties of the production of Si isotopes in the SN models considered here, especially at the bottom of the O/nova zone, the shifts toward heavier Si as plotted in Figure 4 might be even smaller than calculated. The Si mainstream line can be considered a good proxy for the Galactic chemical evolution of Si isotopes because only small modifications of the initial Si-isotopic compositions of the parent AGB stars of SiC mainstream grains are predicted for the third dredge-up events (Zinner et al. 2006; Cristallo et al. 2015). The approximately solar to higher than solar ^{29,30}Si/^{28}Si ratios of mainstream grains, which are older than our solar system, point to AGB parent stars with about solar or supersolar metallicities (Lugaro et al. 2018), a problem that is not finally settled yet. The fact that AB grains show a similar range of Si-isotopic compositions as mainstream grains suggests similar Si starting compositions of the parent stars and only minor modifications during stellar evolution, as predicted by our SN mixing models. This could imply that the AGB stars and SNe that supplied presolar grains had a similar range of initial compositions. This idea is supported by astronomical observations that show that

there was essentially no evolution of metallicity in the Milky Way disk during the last 6–7 Gyr (see Lewis et al. 2013).

Decay of radioactive ^{32}Si (half-life 153 yr) has been invoked to explain the ^{32}S excesses observed in SiC SN grains (Pignatari et al. 2013). Evidence for radiogenic ^{32}S has been reported for some AB grains (Fujiya et al. 2013; Liu et al. 2017a). In the SN models considered here, neutron-capture reactions are mitigated due to the presence of H in the He-burning shell, and the predicted ^{32}Si/^{28}Si ratios are generally low in mixing scenarios SM1-5. Therefore, the missing ^{32}S excesses in AB grains reported here are consistent with our mixing models. We note, however, that S contamination, which is often observed on or around presolar SiC grains and which cannot be reliably identified in ion images, may mask intrinsic S isotope anomalies. For this reason, measured S-isotopic compositions may not be very diagnostic, and we therefore do not discuss them in greater detail here.

4.4. The Diagnostics of Isotopic Compositions of Heavy Elements

As we have shown above, C-, N-, Al-, and Si-isotopic compositions of AB1 and AB2 grains are qualitatively consistent with origins from SNe. In the following, we investigate to which extent our SN mixing models predict signatures of s-process nucleosynthesis in AB grains. Molybdenum, an element that is heavily affected by the s-process, was measured in a large number of presolar SiC grains, including AB grains (Liu et al. 2017b, 2018; Stephan et al. 2019). Here, we explore the ^{100}Mo/^{96}Mo ratio and how it relates to the ^{14}N/^{15}N ratios in our SN mixing models. Molybdenum-100 is essentially a pure r-process isotope, and ^{96}Mo is a pure s-process isotope (Stephan et al. 2019). The He-burning shells of massive stars are expected to show imprints of a mild s-process from the pre-SN phase (Rauscher et al. 2002), and of the n-process from explosive nucleosynthesis (Pignatari et al. 2018). This results in low ^{100}Mo/^{96}Mo ratios in the He/C zone and strongly enhanced ^{100}Mo/^{96}Mo ratios at the bottom of the O/nova zone. Integrating over the whole O/nova and He/C zones yields a lower than solar ^{100}Mo/^{96}Mo ratio; e.g., in model 25T-H10, the ^{100}Mo/^{96}Mo ratio of the combined O/nova and He/C zones is 0.32, compared to the solar ratio of 0.584 (Meija et al. 2016). Predicted ^{100}Mo/^{96}Mo and ^{14}N/^{15}N ratios of our mixing models SM1 and SM2 are displayed in Figure 6. As can be seen from Figure 6, ^{100}Mo/^{96}Mo ratios are positively correlated with ^{14}N/^{15}N ratios. This is because mixtures with low ^{14}N/^{15}N require a higher contribution from the combined O/nova and He/C zones, which leads to lower ^{100}Mo/^{96}Mo ratios. The ^{100}Mo depletion decreases with increasing H concentration in models 25T-Hx (Figure 6). Mixtures with ^{14}N/^{15}N ratios characteristic of AB2 grains are expected to have Mo isotope anomalies of at most a few percent, while for ^{14}N/^{15}N ratios characteristic of AB1 grains, Mo isotope anomalies may reach several 10% (Figure 6).

Almost half of AB1 grains show clearly lower than solar ^{100}Mo/^{96}Mo (Liu et al. 2018), in qualitative agreement with the predictions from our SN mixing models; however, the data do not show a positive correlation between ^{100}Mo/^{96}Mo and ^{14}N/^{15}N, as would be expected (Figure 6). Molybdenum contamination of presolar SiC grains cannot be excluded (Stephan et al. 2019); however, to which extent grains with normal Mo are affected by Mo contamination is not known. Only two out of 13 AB2 grains show strong depletions in
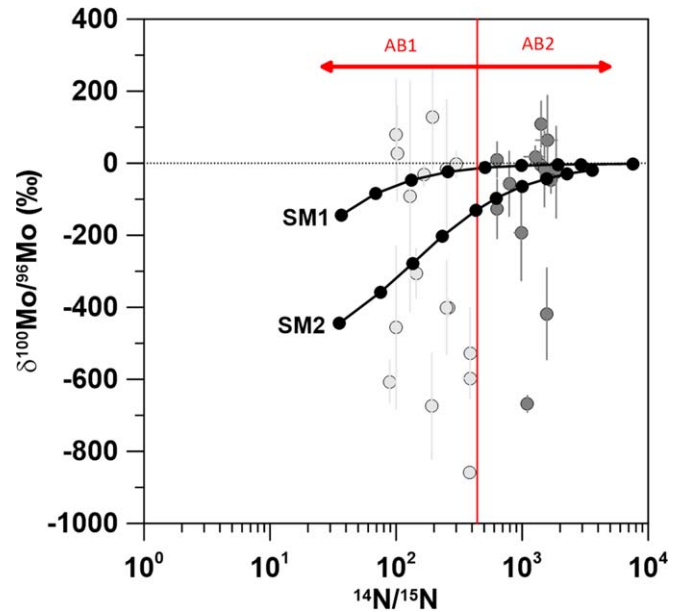

Figure 6. Predictions for δ^{100}Mo/^{96}Mo as a function of ^{14}N/^{15}N for the two SN mixing models from Figure 2 considering the envelope composition of a 25 $M_\odot$ SN (models MS1 and MS2). The red vertical line separates AB1 grains from AB2 grains. Molybdenum- and N-isotopic data of AB1 and AB2 grains are from Liu et al. (2017b, 2018) and Stephan et al. (2019). Errors are 1σ.

^{100}Mo. The ^{100}Mo/^{96}Mo ratios of the others are not much different from the solar ratio (Liu et al. 2017b; Stephan et al. 2019; Figure 6), in agreement with the predictions from our SN mixing models. From this and from the isotopic compositions of C, N, Al, and Si, we conclude that SNe must also be considered potential sources of AB2 grains with only small isotopic anomalies of heavy elements, in addition to J-type C stars and possibly also post-AGB stars. The two AB2 grains with strong depletions in ^{100}Mo (s-process signature) might be from born-again AGB stars that preserved s-process signatures from the preceding AGB phase and experienced only mild or no i-process production following the H ingestion, or from massive stars of lower initial mass than what we considered here and weak SN explosion energy, where we expect a more efficient s-process in the He shell.

4.5. J-type C Stars versus Supernovae as Sources of AB2 Grains

From the discussion above, an open question that we still cannot answer is how to distinguish AB2 grains from J-type C stars from those from SNe, based on isotopic compositions. We believe that this is beyond the capability of currently available models. Not much is known about the evolution of and nucleosynthesis in J-type C stars (see Introduction), and we have seen that the SN models used here have relevant limitations in terms of the capability of fully capturing the stellar structure feedback and the nucleosynthesis output of H-ingestion events. While current SN models are useful for exploring qualitative trends, multi-dimensional and self-consistent SN models with consideration of H ingestion into the He-burning shell will allow us to make a more quantitative comparison between model predictions and the isotope data of AB grains.

An alternative approach to distinguishing AB2 grains from J-type C stars from those from SNe might be to examine the

dust production efficiencies of these stellar sources. AGB stars are considered the most important source of stardust (Gail & Hoppe 2010). As pointed out by Liu et al. (2017b), J-type C stars make up about 10%–15% of all C-rich AGB stars (Abia & Isern 2000), but their dust production efficiency is unknown. In addition to AGB stars, SNe also produce significant amounts of dust (Sugerman et al. 2006; Sarangi et al. 2018), but again, their dust production efficiency is not well constrained. Therefore it is currently not possible to derive a reliable ratio of SiC dust production in the winds of J-type C stars to that in CCSN ejecta.

Among the different types of presolar grains, the inferred contributions of SN grains are 100% for (rare) Si_3N_4 grains, ~25% for graphite, >20% for oxides/silicates, and only ~4% for SiC grains (X, C, and AB1 grains; Hoppe 2016; Leitner & Hoppe 2019). Apparently, the inferred abundance of SN grains among presolar SiC is distinctly lower than for the other presolar grain types. This raises the question whether additional SN grains might be hidden among the different populations of presolar SiC grains. If at least some AB2 grains had an SN origin, the SN contribution to presolar SiC grains could be as high as >5%. Quantitative models of carbonaceous dust production around born-again AGB stars, J-type C stars, and SNe are required to provide additional constraints on the relative contribution of stellar sources to the population of AB2 grains.

5. Summary and Conclusions

We here presented high-resolution C, N, Al, Si, and S isotope data of 38 presolar SiC grains of type AB. The $^{12}C/^{13}C$ ratios of the AB grains in this study are between 1.6 and 16, the $^{14}N/^{15}N$ ratios range from 36 to 10,000, and the $^{26}Al/^{27}Al$ ratios are between 10^{-4} and 0.13. Seventeen of the grains are of subtype AB1 ($^{14}N/^{15}N < 440 =$ solar) and 20 of subtype AB2 ($^{14}N/^{15}N \geqslant 440$); one grain could not be assigned to one of the subtypes because we lack N isotope data. Silicon-isotopic compositions fall along the SiC mainstream line, and the inferred slopes of AB1 and AB2 grains are compatible with the slope of mainstream grains. Sulfur-isotopic compositions are solar within 2σ uncertainties. The data are compatible with previously obtained isotope data of AB grains, with the exception that $^{26}Al/^{27}Al$ ratios of AB1 grains span a narrower range.

A comparison with three SN models of Pignatari et al. (2015), who considered H ingestion into the He shell during the pre-SN phase with H concentrations between 0.06% and 1.2%, shows that the isotopic compositions of AB1 and AB2 grains can be qualitatively matched when matter from the O/nova and He/C zones is mixed with matter from the envelope and when stellar masses between $12\,M_\odot$ and $25\,M_\odot$ are considered. For AB1 grains, this confirms the conclusions drawn by Liu et al. (2017a). For AB2 grains, Liu et al. (2017b) favored an origin from J-type C stars. We have shown here that SNe should be considered as potential sources of a significant fraction of AB2 grains as well, and that born-again AGB stars might also have contributed to the population of AB2 grains.

Because our SN mixing models predict isotopic signatures as observed for J-type C stars (C, N, no s-process) it is currently difficult to distinguish between these two types of stellar sources as suppliers of AB2 grains. It is hoped that future modeling of J-type C stars (and born-again AGB stars) as well as improved, i.e., self-consistent and multi-dimensional SN models with H

ingestion into the He-burning shell will allow us to shed more light on this issue. Both J-type C stars and SNe are considered important suppliers of dust, with relative contributions that are currently not known. Quantitative models of carbonaceous dust production around different types of stellar sources could provide additional constraints on the origin of AB grains.

ORCID iDs

Peter Hoppe ⓘ https://orcid.org/0000-0003-3681-050X
Richard J. Stancliffe ⓘ https://orcid.org/0000-0002-6972-9655
Marco Pignatari ⓘ https://orcid.org/0000-0002-9048-6010

References

Abia, C., & Isern, J. 2000, ApJ, 536, 438
Amari, S., Gao, X., Nittler, L. R., & Zinner, E. 2001a, ApJ, 551, 1065
Amari, S., Hoppe, P., Zinner, E., & Lewis, R. S. 1992, ApJL, 394, L43
Amari, S., Lewis, R. S., & Anders, E. 1994, GeCoA, 58, 459
Amari, S., Nittler, L. R., Zinner, E., Lodders, K., & Lewis, R. S. 2001b, ApJ, 559, 463
Bernatowicz, T., Fraundorf, G., Ming, T., et al. 1987, Natur, 330, 728
Besmehn, A., & Hoppe, P. 2003, GeCoA, 67, 4693
Clarkson, O., Herwig, F., Andrassy, R., et al. 2018, arXiv:1810.12259
Cristallo, S., Straniero, O., Piersanti, L., & Gobrecht, D. 2015, ApJS, 219, 40
Denissenkov, P. A., Truran, J. W., Pignatari, M., et al. 2014, MNRAS, 442, 2058
Denissenkov, P. A., Herwig, F., Woodward, P., et al. 2019, MNRAS, 488, 4258
Fujiya, W., Hoppe, P., Zinner, E., Pignatari, M., & Herwig, F. 2013, ApJL, 776, L29
Gail, H.-P., & Hoppe, P. 2010, in Protoplanetary Dust, ed. D. Apai & D. S. Lauretta (Cambridge: Cambridge Univ. Press), 27
Groopman, E., Zinner, F., Amari, S., et al. 2015, ApJ, 809, 31
Gyngard, F., Jadhav, M., Nittler, L. R., Stroud, R. M., & Zinner, E. 2018, GeCoA, 221, 60
Gyngard, F., Nittler, L. R., & Zinner, E. 2010, M&PS, 45, A72
Hedrosa, R. P., Abia, C., Busso, M., et al. 2013, ApJL, 768, L11
Herwig, F. 2005, ARA&A, 43, 435
Herwig, F., Woodward, P. R., Lin, P.-H., Knox, M., & Fryer, C. 2014, ApJL, 792, L3
Herwig, F., Pignatari, M., Woodward, P. R., et al. 2011, ApJ, 727, 89
Hoppe, P. 2016, in Handbook of Supernovae, ed. A. W. Alsabti & P. Murdin (Berlin: Springer),
Hoppe, P., Amari, S., Zinner, E., Ireland, T., & Lewis, R. S. 1994, ApJ, 430, 870
Hoppe, P., Leitner, J., Gröner, E., et al. 2010, ApJ, 719, 1370
Hoppe, P., Leitner, J., & Kodolányi, J. 2018a, ApJ, 869, 47

Hoppe, P., Pignatari, M., & Amari, S. 2019a, in 50th Lunar and Planetary Science Conf. (Houston, TX: Lunar and Planetary Institute)

Hoppe, P., Pignatari, M., & Amari, S. 2019b, in Nuclei in the Cosmos XV, Vol. 219, ed. A. Formicola et al. (Cham: Springer),

Hoppe, P., Pignatari, M., Kodolányi, J., Gröner, E., & Amari, S. 2018b, GeCoA, 221, 182

Hoppe, P., Strebel, R., Eberhardt, P., Amari, S., & Lewis, R. S. 1996a, GeCoA, 60, 883

Hoppe, P., Strebel, R., Eberhardt, P., Amari, S., & Lewis, R. S. 1996b, Sci, 272, 1314

Hoppe, P., Strebel, R., Eberhardt, P., Amari, S., & Lewis, R. S. 2000, M&PS, 35, 1157

Hoppe, P., Annen, P., Strebel, R., et al. 1997, ApJL, 487, L101

Huss, G. R., Hutcheon, I. D., & Wasserburg, G. J. 1997, GeCoA, 61, 5117

Hynes, K. M., & Gyngard, F. 2009, in 40th Lunar and Planetary Science Conf. (Houston, TX: Lunar and Planetary Institute), 1198

Jose, J., & Hernanz, M. 1998, ApJ, 494, 680

José, J., & Hernanz, M. 2007, M&PS, 42, 1135

Käppeler, F., Gallino, R., Bisterzo, S., & Aoki, W. 2011, RvMP, 83, 157

Leitner, J., & Hoppe, P. 2019, NatAs, 3, 725

Lewis, K. M., Lugaro, M., Gibson, B. K., & Pilkington, K. 2013, ApJL, 768, L19

Lewis, R. S., Amari, S., & Anders, E. 1994, GeCoA, 58, 471

Lin, Y., Amari, S., & Pravdivtseva, O. 2002, ApJ, 575, 257

Lin, Y., Gyngard, F., & Zinner, E. 2010, ApJ, 709, 1157

Liu, N., Nittler, L. R., Alexander, C. M. O. D., et al. 2016, ApJ, 820, 140

Liu, N., Nittler, L. R., Pignatari, M., Alexander, C. M. O. D., & Wang, J. 2017a, ApJL, 842, L1

Liu, N., Stephan, T., Boehnke, P., et al. 2017b, ApJL, 844, L12

Liu, N., Stephan, T., Boehnke, P., et al. 2018, ApJL, 855, 144

Liu, N., Stephan, T., Cristallo, S., et al. 2019, ApJ, 881, 28

Lugaro, M., Karakas, A. I., Petõ, M., & Plachy, E. 2018, GeCoA, 221, 6

Mahon, K. I. 1996, IGRv, 38, 293

Marhas, K. K., Amari, S., Gyngard, F., Zinner, E., & Gallino, R. 2008, ApJ, 689, 622

Marty, B., Chaussidon, M., Wiens, R. C., Jurewicz, J. G., & Burnett, D. S. 2011, Sci, 332, 1533

Meija, J., Coplen, T. B., Berglund, M., et al. 2016, PApCh, 88, 293

Messenger, S., Keller, L. P., Stadermann, F., Walker, R. M., & Zinner, E. 2003, Sci, 300, 105

Nittler, L. R. 1996, PhD thesis, Washington Univ., St. Louis

Nittler, L. R., Alexander, C. M. O. D., Liu, N., & Wang, J. 2018, ApJL, 856, L24

Nittler, L. R., Amari, S., Zinner, E., Woosley, S. E., & Lewis, R. S. 1996, ApJL, 462, L31

Nittler, L. R., & Hoppe, P. 2005, ApJL, 631, L89

Ohnaka, K., & Tsuji, T. 1999, A&A, 345, 233

Pignatari, M., Hoppe, P., Trappitsch, R., et al. 2018, GeCoA, 221, 37

Pignatari, M., Zinner, E., Bertolli, M. G., et al. 2013, ApJL, 771, L7

Pignatari, M., Zinner, E., Hoppe, P., et al. 2015, ApJL, 808, L43

Pignatari, M., Herwig, F., Hirschi, R., et al. 2016, ApJS, 225, 24

Rauscher, T., Heger, A., Hoffman, R. D., & Woosley, S. E. 2002, ApJ, 576, 323

Sarangi, A., Matsuura, M., & Micelotta, E. R. 2018, SSRv, 214, 63

Sengupta, S., Izzard, R. G., & Lau, H. H. B. 2013, A&A, 559, A66

Stancliffe, R. J., Dearborn, D. S. P., Lattanzio, J. C., Heap, S. A., & Campbell, S. W. 2011, ApJ, 742, 121

Stephan, T., Trappitsch, R., Hoppe, P., et al. 2019, ApJ, 877, 101

Sugerman, B. E. K., et al. 2006, Sci, 313, 196

Wiescher, M., Görres, J., Uberseder, E., Imbriani, G., & Pignatari, M. 2010, ARNPS, 60, 381

Woodward, P. R., Herwig, F., & Lin, P.-H. 2015, ApJ, 798, 49

Woosley, S. E., & Heger, A. 2007, PhR, 442, 269

Xu, Y., Zinner, E., Gallino, R., et al. 2015, ApJ, 799, 156

York, D. 1969, E&PSL, 5, 320

Zinner, E. 2014, in Meteorites and Cosmochemical Processes, ed. A. M. Davis (Amsterdam: Elsevier), 181

Zinner, E., Nittler, L. R., Gallino, R., et al. 2006, ApJ, 650, 350

Zinner, E., Amari, S., Guinness, R., et al. 2007, GeCoA, 71, 4786